



## A novel potent class I HDAC inhibitor reverses the STAT4/p66Shc apoptotic defect in B cells from chronic lymphocytic leukemia patients

Sara Rossi<sup>a,1</sup>, Vanessa Tatangelo<sup>b,1</sup>, Maria Dichiarà<sup>a</sup>, Stefania Butini<sup>a</sup>, Sandra Gemma<sup>a</sup>, Simone Brogi<sup>c</sup>, Silvia Pasquini<sup>d</sup>, Martina Cappello<sup>e</sup>, Fabrizio Vincenzi<sup>e</sup>, Katia Varani<sup>e</sup>, Ludovica Lopresti<sup>b</sup>, Margherita Malchiodi<sup>f</sup>, Chiara Carrara<sup>f</sup>, Alessandro Gozzetti<sup>f</sup>, Monica Bocchia<sup>f</sup>, Giuseppe Marotta<sup>g</sup>, Laura Patrussi<sup>b,\*</sup>, Gabriele Carullo<sup>a,\*\*</sup>, Cosima T. Baldari<sup>b</sup>, Giuseppe Campiani<sup>a,h</sup>

<sup>a</sup> Department of Biotechnology, Chemistry and Pharmacy, University of Siena, Via Aldo Moro 2, Siena 53100, Italy

<sup>b</sup> Department of Life Sciences, University of Siena, Via Aldo Moro 2, Siena 53100, Italy

<sup>c</sup> Department of Pharmacy, University of Pisa, Via Bonanno, Pisa 56126, Italy

<sup>d</sup> Department of Chemical, Pharmaceutical and Agricultural Sciences, University of Ferrara, Via Borsari 46, Ferrara 44121, Italy

<sup>e</sup> Department of Translational Medicine, University of Ferrara, Via Borsari 46, Ferrara 44121, Italy

<sup>f</sup> Haematology Unit, Department of Medical Sciences, Surgery and Neuroscience, University of Siena, Policlinico "Santa Maria alle Scotte", Viale Bracci, Siena 53100, Italy

<sup>g</sup> Stem Cell Transplant and Cellular Therapy Unit, University Hospital, Policlinico "Santa Maria alle Scotte", Viale Bracci, Siena 53100, Italy

<sup>h</sup> Bioinformatics Research Center, School of Pharmacy and Pharmaceutical Sciences, Isfahan University of Medical Sciences, Isfahan 81746-7346, Iran

### ARTICLE INFO

#### Keywords:

Chronic lymphocytic leukemia  
p66Shc  
HDAC inhibitors  
STAT4  
HDAC1  
chlopynostat  
blood malignancies

### ABSTRACT

Chronic Lymphocytic Leukemia (CLL) patients have a defective expression of the proapoptotic protein p66Shc and of its transcriptional factor STAT4, which evoke molecular abnormalities, impairing apoptosis and worsening disease prognosis and severity. p66Shc expression is epigenetically controlled and transcriptionally modulated by STAT4; epigenetic modifiers are deregulated in CLL cells and specific histone deacetylases (HDACs) like HDAC1, are overexpressed. Reactivation of STAT4/p66Shc expression may represent an attractive and challenging strategy to reverse CLL apoptosis defects. New selective class I HDAC inhibitors (HDACis, **6a-g**) were developed with increased potency over existing agents and preferentially interfering with the CLL-relevant isoform HDAC1, to unveil the role of class I HDACs in the upregulation of STAT4 expression, which upregulates p66Shc expression and hence normalizes CLL cell apoptosis. **6c** (chlopynostat) was identified as a potent HDAC1i with a superior profile over entinostat. **6c** induces marked apoptosis of CLL cells compared with SAHA, which was associated with an upregulation of STAT4/p66Shc protein expression. The role of HDAC1, but not HDAC3, in the epigenetic upregulation of STAT4/p66Shc was demonstrated for the first time in CLL cells and was validated in siRNA-induced HDAC1/HDAC3 knock-down EBV-B cells. To sum up, HDAC1 inhibition is necessary to reactivate STAT4/p66Shc expression in patients with CLL. **6c** is one of the most potent HDAC1is known to date and represents a novel pharmacological tool for reversing the impairment of the STAT4/p66Shc apoptotic machinery.

**Abbreviations:** BCL-2, B-cell lymphoma 2; BTK, Bruton tyrosine kinase; CAP, surface recognition group; CLL, Chronic Lymphocytic Leukemia; DIPEA, *N,N*-Diisopropylethylamine; DMSO, dimethyl sulfoxide; ESI, electron spray ionization; EtOAc, ethyl acetate; HBTU, hexafluorophosphate Benzotriazole Tetramethyl Uranium; HDAC, histone deacetylase; IL-12, interleukin-12; NMR, nuclear magnetic resonance; PDB, Protein Data Bank; Ppm, parts per million; TLC, thin-layer chromatography; ZBG, zinc-binding group.

\* Correspondence to: Department of Life Sciences, Via Aldo Moro 2, Siena 53100, Italy.

\*\* Correspondence to: Department of Biotechnology, Chemistry and Pharmacy, Via Aldo Moro 2, Siena 53100, Italy.

E-mail addresses: [patrussi2@unisi.it](mailto:patrussi2@unisi.it) (L. Patrussi), [gabriele.carullo@unisi.it](mailto:gabriele.carullo@unisi.it) (G. Carullo).

<sup>1</sup> co-first authors

<https://doi.org/10.1016/j.bioph.2024.116537>

Received 12 January 2024; Received in revised form 20 March 2024; Accepted 29 March 2024

Available online 4 April 2024

0753-3322/© 2024 The Author(s). Published by Elsevier Masson SAS. This is an open access article under the CC BY-NC-ND license (<http://creativecommons.org/licenses/by-nc-nd/4.0/>).

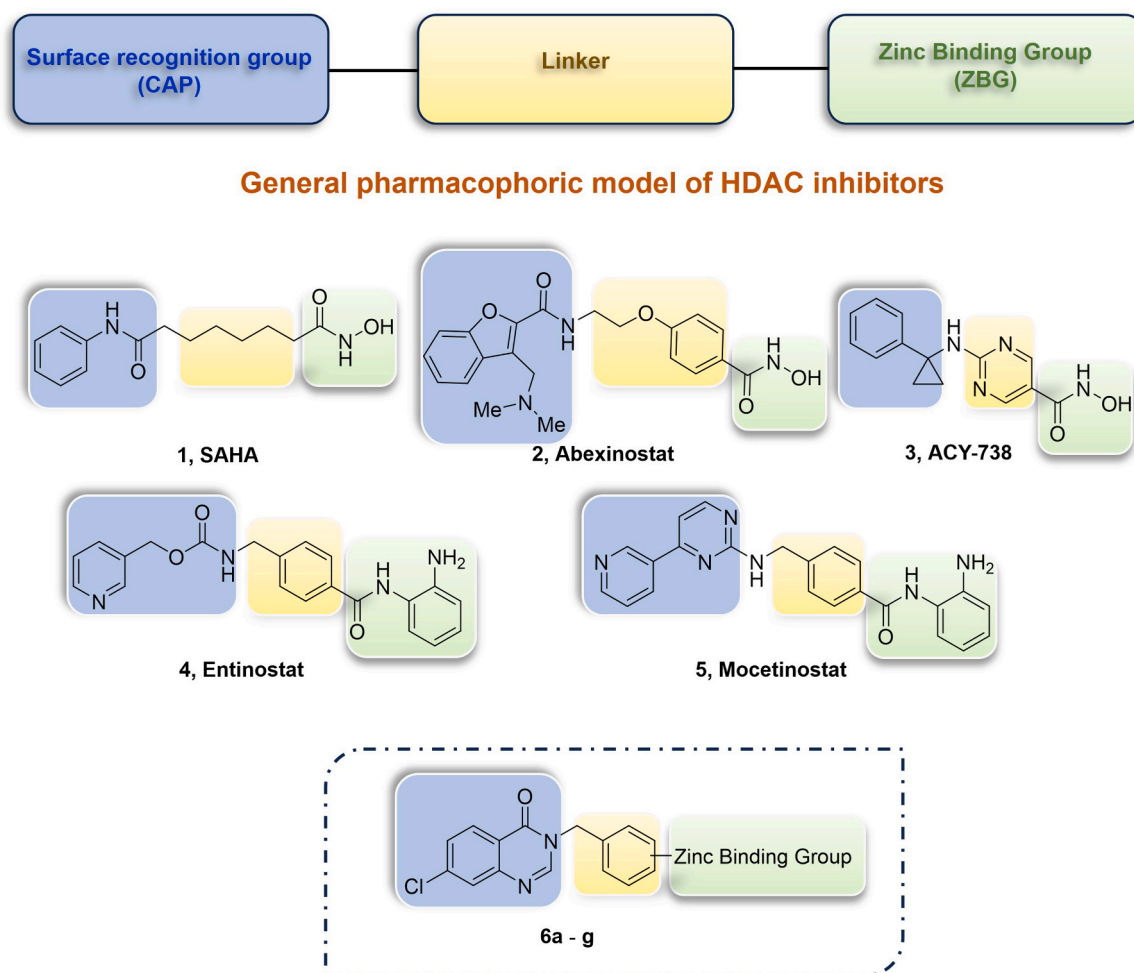


Fig. 1. Known HDAC inhibitors acting as antitumor agents in CLL and general structure of the target HDAC inhibitors 6a-g.

## 1. Introduction

Chronic Lymphocytic Leukemia (CLL) is the most common type of leukemia in the elderly. The incidence of CLL is approximately 4.9 per 100,000 inhabitants per year, with a median age at diagnosis of 70 years, although 9.1% of CLL patients are younger than 45 years [1]. Current treatments include the B-cell lymphoma 2 (BCL-2) inhibitor venetoclax and the monoclonal anti-CD20 antibody obinutuzumab. Other options include monotherapy with Bruton tyrosine kinase (BTK) inhibitors such as ibrutinib and acalabrutinib or chemoimmunotherapy. This latter approach has several drawbacks, including a low efficacy in cohorts of patients, the potential for the emergence of aggressive clones, and a significant economic burden [2].

CLL is associated with the accumulation of CD5<sup>+</sup> B cells in peripheral blood and lymphoid organs. The majority of patients carry at least one of four typical chromosomal alterations, namely deletions in chromosomes 13 (del[13q]), 11 (del[11q]), 17 (del[17p]), or trisomy 12. Furthermore, the genomic and epigenomic landscape shows abnormalities in patients with CLL [3]. In particular, deletions and mutations in the TP53 gene are found in approximately 10% of patients at the time of initial diagnosis, resulting in an aggressive and often refractory phenotype with poor response to therapies [4].

In CLL, aberrant accumulation of leukemic cells is mainly due to impaired apoptosis, which has been partly ascribed to a profound defect in the expression of p66Shc, a pro-apoptotic adaptor whose expression in certain tissues is epigenetically regulated [5]. Impairment in p66Shc expression contributes to prolonging leukemic cell survival by modulating the balance of the BCL-2 family of apoptosis-regulating proteins

toward the pro-survival BCL-2 and BCL2L1 members [6,7].

The expression of p66Shc is regulated by the transcription factor STAT4 [8], a crucial mediator of interleukin-12 (IL-12)-mediated signaling [9]. Interestingly, STAT4 expression is also defective in CLL cells, accounting for the p66Shc deficiency of CLL cells [8].

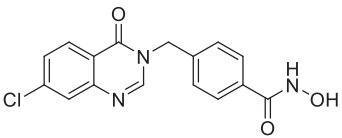
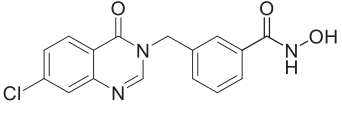
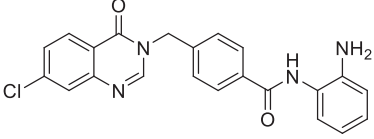
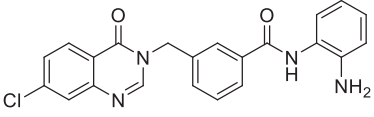
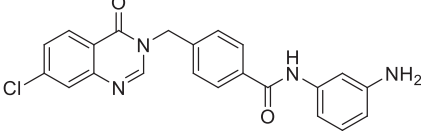
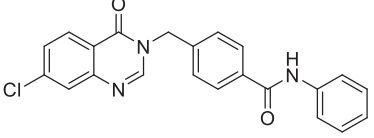
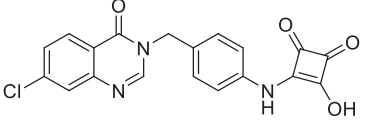
IL-12-dependent STAT4 activation or STAT4 reconstitution by transient transfection causes a coordinated increase in STAT4 and p66Shc expression, which correlates with enhanced CLL cell apoptosis [8]. Hence, pharmacological strategies aimed at enhancing STAT4 expression in CLL cells may lead to upregulation of p66Shc expression and reverse the apoptosis defects caused by p66Shc deficiency.

STAT4 expression is increased in Cutaneous T-cell Lymphoma cells treated *in vitro* with the *pan*-HDAC inhibitor vorinostat (SAHA, 1, Fig. 1) [10], suggesting that HDACs are promising and explorable molecular targets to promote STAT4 expression.

Interestingly, both the expression and activity of the HDAC iso-enzymes HDAC1 and HDAC3 (class I), and HDAC6 (class II) are enhanced in CLL cells, and their aberrant activation has been related to poor disease prognosis [11,12]. The critical implications of HDAC iso-form overexpression and aberrant activation in CLL are witnessed by the recent entry of the *pan*-HDAC inhibitor abexinostat (2, Fig. 1) in clinical trials for T-cell lymphoma and CLL [13].

More recently, the treatment of Eμ-TCL1 mice, a mouse model of CLL [14], with the HDAC1/6 inhibitor ACY-738 (3, Fig. 1) led to a reduction of immunosuppression and amelioration of disease outcome [15]. Moreover, the *pan*-HDAC inhibitors entinostat (4, MS-275-see Table 1 for IC<sub>50</sub>s) and mocetinostat (5, MGCD0103 HDAC1 IC<sub>50</sub> = 150 nM) (Fig. 1) have been found to promote CLL cell apoptosis.

**Table 1**  
Inhibitory activity of compounds **6a-g** against hHDAC1, hHDAC6, hHDAC8 and hHDAC10 (as IC<sub>50</sub>, nM).

Cpds	Structure	IC <sub>50</sub> (nM)			
		hHDAC1	hHDAC6	hHDAC8	hHDAC10
<b>6a</b>		890 ± 61	9.6 ± 0.68	707 ± 44	1116 ± 76
<b>6b</b>		1188 ± 82	1077 ± 73	3263 ± 196	>10,000
<b>6c</b>		67 ± 4	>10,000	>10,000	1149 ± 76
<b>6d</b>		>10,000	NT	NT	NT
<b>6e</b>		>10,000	NT	NT	NT
<b>6f</b>		>10,000	NT	NT	NT
<b>6g</b>		>10,000	>10,000	>10,000	>10,000
<b>4</b>		1231 ± 83	>10,000	NT	3127 ± 231

Data are expressed as mean ± SEM of three independent experiments performed in triplicate. Data in parentheses indicates inhibition at the 10,000 nM concentration. Incubation time = 30 min. NT: not tested.

Hence, starting from the hypothesis that inhibition of HDAC1, overexpressed in CLL cells, may recover CLL cell apoptosis by normalizing STAT4/p66Shc expression, we herein describe the development of a highly focused small set of HDAC modulators to achieve a significant potency for class I HDACs, preferentially inhibiting the CLL relevant isoform HDAC1, over other specific isoforms (HDAC6/8/10). We moreover describe the identification of a novel pharmacological tool to investigate whether HDAC1 inhibition could revert the STAT4/p66Shc-dependent apoptosis defects in CLL cells from patients.

7-Chloroquinazolin-4(3H)-one was selected as a key surface recognition scaffold to synthesize a small library of isozyme-selective HDAC inhibitors (**6a-g**, Fig. 1, Table 1). **6a-g** were tested *in vitro* to measure their HDAC inhibition profile and were assayed in leukemic cells from CLL patients to investigate their effect on the reactivation of the STAT4/p66Shc apoptotic pathway.

## 2. Material and methods

### 2.1. General chemistry information

All reagents were purchased from commercial suppliers and used without further purification. All moisture-sensitive reactions were performed under a nitrogen atmosphere using oven-dried glassware and anhydrous solvents. Flash column chromatography was carried out on silica gel (Merck: Kieselgel 60, particle size 0.040–0.063 mm). Reactions' progression was monitored by thin-layer chromatography (TLC), carried out using glass-backed plates coated with Merck Kieselgel 60 GF254. Plates were visualized under UV light (at 254 nm) or by staining with potassium permanganate, ninhydrin followed by heating. <sup>1</sup>H NMR and <sup>13</sup>C NMR spectra were recorded on a Varian 300 MHz spectrometer using the residual signal of the deuterated solvent as an internal standard. Coupling constants (*J*) are given in hertz (Hz). Splitting patterns are described as singlet (s), doublet (d), triplet (t), quartet (q), and broad (br); the value of chemical shifts ( $\delta$ ) are given in parts per million (ppm). Mass spectra were recorded utilizing an electron spray

ionization (ESI) Agilent 1100 Series LC/MSD spectrometer. Yields refer to purified products and are not optimized.

## 2.2. Synthesis of compounds 8a,b

To a well-stirred solution of **7** (250 mg, 1.26 mmol) in acetone (15 mL), methyl 4-(bromomethyl)benzoate (for **8a**) or methyl 3-(bromomethyl)benzoate (for **8b**), K<sub>2</sub>CO<sub>3</sub> (867 mg, 6.28 mmol) and NaI (188 mg, 1.26 mmol) were added. The mixture was stirred at 55 °C for 12 h. The mixture was then filtered, the solvent was removed and the pure compound was crystallized from *n*-hexane.

### 2.2.1. Methyl 4-((7-chloro-4-oxoquinazolin-3(4H)-yl)methyl)benzoate (8a)

Yellow solid, 96% yield. ESI-MS *m/z* 329 [M+H]<sup>+</sup>, 351 [M+Na]<sup>+</sup>. <sup>1</sup>H NMR (300 MHz, DMSO-*d*<sub>6</sub>) δ 8.63 (s, 1H), 8.11 (d, *J* = 8.5 Hz, 1H), 8.00 – 7.85 (m, 2H), 7.76 (d, *J* = 2.0 Hz, 1H), 7.58 (d, *J* = 2.0 Hz, 1H), 7.46 (d, *J* = 8.4 Hz, 2H), 5.25 (s, 2H), 3.81 (s, 3H).

### 2.2.2. Methyl 3-((7-chloro-4-oxoquinazolin-3(4H)-yl)methyl)benzoate (8b)

White solid, 93% yield. ESI-MS *m/z* 329 [M+H]<sup>+</sup>, 351 [M+Na]<sup>+</sup>. <sup>1</sup>H NMR (300 MHz, CDCl<sub>3</sub>) δ 8.21 (d, *J* = 8.6 Hz, 1H), 8.13 (s, 1H), 8.07 – 7.88 (m, 2H), 7.68 (d, *J* = 2.0 Hz, 1H), 7.55 (dt, *J* = 7.9, 1.5 Hz, 1H), 7.51 – 7.37 (m, 2H), 5.20 (s, 2H), 3.89 (d, *J* = 1.6 Hz, 3H).

### 2.2.3. 3-(4-Aminobenzyl)-7-chloroquinazolin-4(3H)-one (8c)

The compound was synthesized as previously reported; spectroscopic data are in agreement with those previously reported [16].

## 2.3. Synthesis of 3-((4-((7-chloro-4-oxoquinazolin-3(4H)-yl)methyl)phenyl)amino)-4-methoxycyclobut-3-ene-1,2-dione (9)

To a well-stirred solution of **8c** (275 mg, 0.96 mmol) in MeOH (10 mL), dimethyl squarate (137 mg, 0.96 mmol) was added. The mixture was stirred at 25 °C for 15 h. Then, it was filtered and the solid was washed with water. Orange solid, 47% yield. ESI-MS *m/z* 396 [M+H]<sup>+</sup>. <sup>1</sup>H NMR (300 MHz, DMSO-*d*<sub>6</sub>) δ 10.75 (s, 1H), 8.61 (s, 1H), 8.12 (d, *J* = 8.5 Hz, 1H), 7.75 (d, *J* = 2.1 Hz, 1H), 7.57 (dd, *J* = 8.6, 2.1 Hz, 1H), 7.32 (q, *J* = 8.4 Hz, 4H), 5.12 (s, 2H), 4.34 (s, 3H).

## 2.4. Synthesis of compounds 6a,b

To a suspension of NH<sub>2</sub>OH·HCl (500 mg, 7.2 mmol) in MeOH (5 mL), a solution of KOH (648 mg, 11.5 mmol) in MeOH (5 mL) was added at 0 °C and stirred for 30 min at 25 °C. Then, the solid residue was filtered off and the filtrate was added to a mixture of **8a** or **8b** (250 mg, 0.76 mmol) in MeOH (5 mL). The resulting solution was stirred at 25 °C for 12 h. After that, pH was neutralized by adding aqueous 6 N HCl. Solvents were removed under reduced pressure and the target compound was purified through silica gel column chromatography, using a mixture of CHCl<sub>3</sub>/MeOH/NH<sub>4</sub>OH (20:1:0.1) as the eluent.

### 2.4.1. 4-((7-Chloro-4-oxoquinazolin-3(4H)-yl)methyl)-*N*-hydroxybenzamide (6a)

Orange solid, 24% yield. ESI-MS *m/z* 330 [M+H]<sup>+</sup>. <sup>1</sup>H NMR (300 MHz, DMSO-*d*<sub>6</sub>) δ 11.18 (s, 1H), 8.63 (s, 1H), 8.12 (d, *J* = 8.6 Hz, 1H), 7.87 – 7.52 (m, 4H), 7.40 (d, *J* = 8.2 Hz, 2H), 5.21 (s, 2H). <sup>13</sup>C NMR (75 MHz, DMSO-*d*<sub>6</sub>) δ 164.2, 160.0, 149.9, 149.5, 140.0, 139.5, 132.6, 129.1, 128.0, 127.6, 126.9, 120.9, 49.3.

### 2.4.2. 3-((7-Chloro-4-oxoquinazolin-3(4H)-yl)methyl)-*N*-hydroxybenzamide (6b)

Yellow solid, 13% yield. ESI-MS *m/z* 330 [M+H]<sup>+</sup>. <sup>1</sup>H NMR (300 MHz, DMSO-*d*<sub>6</sub>) δ 11.22 (s, 2H), 9.03 (s, 1H), 8.64 (s, 1H), 8.13 (d, *J* = 8.5 Hz, 1H), 7.93 – 7.25 (m, 6H), 5.21 (s, 2H).

## 2.5. Synthesis of compounds 6c-f

To a well-stirred solution of **8a,b** (395 mg, 1.20 mmol) in THF (20 mL), aqueous NaOH (192 mg, 4.80 mmol) was added. The mixture was stirred at 25 °C for 12 h. Then, the mixture was neutralized with 6 N HCl and extracted with EtOAc. The organic layer was then dried, filtered and evaporated under vacuum. Without any further purification, the carboxylic acid (380 mg, 1.20 mmol) was solubilized in dry DMF (15 mL) and suitable aniline (*o*-phenylenediamine for **6c** and **6d**, *m*-phenylenediamine for **6e**, aniline for **6f**) (0.8 eq.), HBTU (551 mg, 1.45 mmol), and TEA (673 μL, 4.84 mmol) were added. The resulting mixture was stirred at 25 °C for 12 h. Then, it was treated with a saturated solution of NH<sub>4</sub>Cl and extracted with EtOAc. The pure compound was obtained after flash-column chromatography (eluent CHCl<sub>3</sub>:MeOH 20:1) and subsequent crystallization from ethanol.

### 2.5.1. *N*-(2-Aminophenyl)-4-((7-chloro-4-oxoquinazolin-3(4H)-yl)methyl)benzamide (6c)

Yellow solid, 73% yield. ESI-MS *m/z* 427 [M+Na]<sup>+</sup>. <sup>1</sup>H NMR (300 MHz, DMSO-*d*<sub>6</sub>) δ 9.62 (s, 1H), 8.66 (s, 1H), 8.13 (d, *J* = 8.6 Hz, 1H), 7.93 (d, *J* = 8.1 Hz, 2H), 7.78 (d, *J* = 2.0 Hz, 1H), 7.59 (dd, *J* = 8.6, 2.1 Hz, 1H), 7.47 (d, *J* = 8.1 Hz, 2H), 7.12 (d, *J* = 7.7 Hz, 1H), 7.05 – 6.85 (m, 1H), 6.75 (dd, *J* = 8.0, 1.4 Hz, 1H), 6.57 (t, *J* = 7.8 Hz, 1H), 5.25 (s, 2H), 4.87 (s, 2H). <sup>13</sup>C NMR (75 MHz, DMSO-*d*<sub>6</sub>) δ 161.6, 160.0, 149.9, 149.5, 143.6, 140.3, 139.6, 134.5, 128.6, 127.9, 127.1, 123.5, 120.9, 116.7, 49.7.

### 2.5.2. *N*-(2-Aminophenyl)-3-((7-chloro-4-oxoquinazolin-3(4H)-yl)methyl)benzamide (6d)

Light orange solid, 67% yield. ESI-MS *m/z* 404 [M+Na]<sup>+</sup>. <sup>1</sup>H NMR (300 MHz, DMSO-*d*<sub>6</sub>) δ 9.66 (s, 1H), 8.66 (s, 1H), 8.14 (d, *J* = 8.6 Hz, 1H), 7.95 (s, 1H), 7.90 (d, *J* = 7.7 Hz, 1H), 7.76 (d, *J* = 1.9 Hz, 1H), 7.61 – 7.53 (m, 2H), 7.47 (t, *J* = 7.6 Hz, 1H), 7.11 (d, *J* = 7.6 Hz, 1H), 6.95 (t, *J* = 7.6 Hz, 1H), 6.75 (d, *J* = 7.9 Hz, 1H), 6.56 (t, *J* = 7.4 Hz, 1H), 5.23 (s, 2H), 4.85 (s, 2H). <sup>13</sup>C NMR (75 MHz, DMSO-*d*<sub>6</sub>) δ 165.5, 160.1, 150.0, 149.5, 143.7, 139.5, 137.2, 135.4, 131.3, 129.1, 128.7, 127.9, 127.6, 127.5, 127.2, 127.0, 126.9, 123.5, 120.9, 116.6, 116.5, 49.4.

### 2.5.3. 3-(3-Aminophenyl)-4-((7-chloro-4-oxoquinazolin-3(4H)-yl)methyl)benzamide (6e)

Brown solid, 41% yield. ESI-MS *m/z* 404 [M+Na]<sup>+</sup>. <sup>1</sup>H NMR (300 MHz, DMSO-*d*<sub>6</sub>) δ 9.90 (s, 1H), 8.65 (s, 1H), 8.13 (d, *J* = 8.6 Hz, 1H), 7.85 (d, *J* = 8.2 Hz, 2H), 7.77 (d, *J* = 1.7 Hz, 1H), 7.58 (dd, *J* = 8.6, 2.0 Hz, 1H), 7.46 (d, *J* = 8.2 Hz, 2H), 7.06 (s, 1H), 6.93 (t, *J* = 7.9 Hz, 1H), 6.83 (d, *J* = 8.1 Hz, 1H), 6.30 (d, *J* = 8.0 Hz, 1H), 5.25 (bs, 4H). <sup>13</sup>C NMR (75 MHz, DMSO-*d*<sub>6</sub>) δ 165.4, 160.0, 149.9, 149.5, 149.0, 140.2, 140.0, 139.5, 135.2, 129.2, 128.7, 128.4, 128.0, 126.9, 120.9, 110.3, 109.0, 106.6, 49.4.

### 2.5.4. 4-((7-Chloro-4-oxoquinazolin-3(4H)-yl)methyl)-*N*-phenylbenzamide (6f)

Yellow solid, 37% yield. ESI-MS *m/z* 390 [M+H]<sup>+</sup>. <sup>1</sup>H NMR (300 MHz, Acetone-*d*<sub>6</sub>) δ 9.47 (s, 1H), 8.23 (s, 1H), 8.06 – 7.77 (m, 3H), 7.56 (dd, *J* = 34.1, 8.2 Hz, 3H), 7.34 (t, *J* = 7.8 Hz, 2H), 7.10 (t, *J* = 7.4 Hz, 1H), 6.84 (d, *J* = 2.1 Hz, 1H), 6.64 – 6.45 (m, 2H), 4.64 (d, *J* = 6.2 Hz, 2H). <sup>13</sup>C NMR (75 MHz, Acetone-*d*<sub>6</sub>) δ 168.4, 165.2, 151.4, 143.5, 139.5, 134.0, 129.3, 128.5, 127.5, 127.3, 123.5, 120.1, 120.0, 115.6, 114.8, 42.5.

### 2.5.5. Synthesis of 3-((4-((7-chloro-4-oxoquinazolin-3(4H)-yl)methyl)phenyl)amino)-4-hydroxycyclobut-3-ene-1,2-dione (6g)

To a well stirred solution of **9** (100 mg, 2.52 mmol), 6 N HCl (3 mL) was added and the mixture heated at 90 °C for 14 h. Then, it was filtered and the solid washed with water. Orange solid, 87% yield. ESI-MS *m/z* 380 [M-H]<sup>-</sup>. <sup>1</sup>H NMR (300 MHz, DMSO-*d*<sub>6</sub>) δ 10.37 (s, 1H), 8.60 (s, 1H), 8.12 (d, *J* = 8.6 Hz, 1H), 7.74 (d, *J* = 2.1 Hz, 1H), 7.57 (dd, *J* = 8.6,



2.1 Hz, 1H), 7.34 (q,  $J = 8.6$  Hz, 4H), 5.11 (s, 2H).  $^{13}\text{C}$  NMR (75 MHz, DMSO- $d_6$ )  $\delta$  188.8, 185.2, 171.6, 160.0, 149.8, 149.4, 139.5, 138.7, 131.6, 129.2, 128.7, 127.9, 126.8, 120.9, 119.4, 48.1.

## 2.6. Human HDAC inhibition assay

For the evaluation of their inhibitory activity, different concentrations of the compounds were incubated in a low-binding black 96-well plate with 30 ng of human recombinant HDAC6 (BPS Bioscience, San Diego, CA, USA; Cat. # 50056), human recombinant HDAC1 (BPS Bioscience; Cat. # 50051), human recombinant HDAC8 (BPS Bioscience; Cat. # 50008), or 500 ng of human recombinant HDAC10 (BPS Bioscience; Cat. # 50060) in an assay buffer composed of 25 mM Tris/HCl, pH 8.0, 137 mM NaCl, 2.7 mM KCl, 1 mM  $\text{MgCl}_2$ , and 0.1 mg/mL bovine serum albumin for 30 min at 37 °C. At the end of the incubation, the deacetylation reaction was initiated by adding 200  $\mu\text{M}$  of the fluorogenic acetylated HDAC substrate 3 (BPS Bioscience; Cat. # 50037) for HDAC6, HDAC1 and HDAC10 assays, or of the fluorogenic HDAC substrate class 2 A (BPS Bioscience; Cat. # 50040) for HDAC8 assays. After 30 min at 37 °C, the reaction was stopped by the addition of an HDAC assay developer (BPS Bioscience; Cat. # 50060). Following an incubation of 15 min at RT, fluorescence was measured in an EnSight multimodal plate reader (PerkinElmer, Boston, MA, USA) with an excitation wavelength of 360 nm and an emission wavelength of 450 nm.

## 2.7. Patients, healthy donors, and cell lines

Peripheral blood samples were collected from 19 treatment-naive CLL patients. CLL was diagnosed according to the international workshop on CLL (iwCLL) 2008 criteria [1]. Primary human B cells from 16 buffy coats were used as healthy population controls. B cells were purified by negative selection using RosetteSep™ B-cell enrichment Cocktail (StemCell Technologies, Vancouver, Canada #15063), followed by density gradient centrifugation on Lympholyte (Cedarlane Laboratories, The Netherlands) according to the manufacturer's instructions. Primary B cells and Epstein-Barr Virus immortalized B cells (EBV-B) were cultured in RPMI-1640 (Sigma-Aldrich, Darmstadt, Germany) supplemented with 7.5% BCS (Bovine Calf Serum, Hyclone, Logan, Utah, USA) at 37 °C in a humidified atmosphere with 5%  $\text{CO}_2$ .

## 2.8. Cell treatments

The compounds were resuspended in sterile dimethyl sulfoxide (DMSO, Merck, Darmstadt, Germany). Cells were treated in complete medium with 1, 2.5 and 5  $\mu\text{M}$  of the indicated compounds for 24 h at 37 °C and 5%  $\text{CO}_2$ , and the control conditions contained the highest amount of DMSO.

## 2.9. Nucleofection, RNA interference and luciferase assays

EBV-B cells were transiently transfected by nucleofection using materials supplied in the Amaxa Cell Line Optimization Nucleofector Kit™ (Amaxa Biosystem, Cologne, Germany).  $5 \times 10^6$  cells were suspended in 100  $\mu\text{L}$  of Cell Line Nucleofector Solution V in an Amaxa-certified cuvette. The esiRNAs used to silence HDAC1 (#EHU025841), HDAC3 (#EHU035581) in EBV-B cells, as well as unrelated control RLuc esiRNA (#EHURLUC) (200 ng/ $10^6$  cells) were purchased from Sigma-Aldrich and assays were carried out after 24 h. For luciferase assays,  $5 \times 10^6$  B cells purified from CLL patients were transiently transfected with 2.5  $\mu\text{g}$  of the *p66shc*-luciferase reporter vector pGL4/*p66Shc* using the Human B-cell Nucleofector Kit (Amaxa Biosystems, Cologne, Germany) as described [8]. 6 h post-transfection,  $1 \times 10^6$  cells were resuspended in 1 mL complete medium and treated for additional 18 h with 5  $\mu\text{M}$  of the indicated compounds. Cells collected after treatment were processed for luciferase assays using the fluoroscan microplate reader Tecan Infinity Pro F200, as described [17]. The luciferase

activity, normalized to the total protein amount quantified by IMarkTM Plate Reader (BioRad) using the Quantum Protein assay kit (Euroclone, #EMP14250), was expressed as Relative Luciferase Units (RLU). All samples were performed in duplicate.

## 2.10. Apoptosis assays and flow cytometry

Apoptosis was measured after 24 h of treatment by flow cytometric analysis of  $1 \times 10^6$  cells co-stained with FITC-labeled Annexin V (Bio-Legend, San Diego, California, USA, #640906) and Propidium Iodide (PI, 0.5  $\mu\text{g}/\text{mL}$ , Millipore, Burlington, Massachusetts, USA, #537059). Data are expressed as percentage of Annexin V<sup>+</sup>/PI<sup>-</sup> early apoptotic cells. Activation of caspase-3 was measured by flow cytometry in  $0.2 \times 10^6$  cells treated as above and then stained for 25 min with 5  $\mu\text{M}$  Nuc-View® 488 Caspase-3 Assay Kit (Biotium, #30029) [18]. Flow cytometry was performed using a Guava Easy Cyte cytometer (Luminex Corporation, Austin, Texas, USA).

## 2.11. RNA Purification and qRT-PCR

Total RNA was extracted using the RNA mini kit (Qiagen, Hilden, Germany), and retrotranscription was carried out using the IScript cDNA synthesis kit (Bio-Rad, Hercules, California, USA), as reported [19]. Real-time quantitative PCR (qRT-PCR) was performed in triplicate using SSo Fast EvaGreenR SuperMix (Bio-Rad) according to the manufacturer's instructions and a CFX96 Real-Time system (Bio-Rad). After an initial denaturation for 3 min at 95 °C, denaturation in the subsequent 40 cycles was performed for 10 s at 95 °C, followed by 30-s primer annealing at 60 °C and a final extension at 72 °C for 30 s. The results were processed and analyzed using CFX Manager Version 1.5 software (Bio-Rad). Transcript levels were normalized to HPRT1 (hypoxanthine phosphoribosyltransferase 1), which was used as a housekeeping gene. The primers used to amplify the cDNA fragments corresponding to human transcripts are listed below:

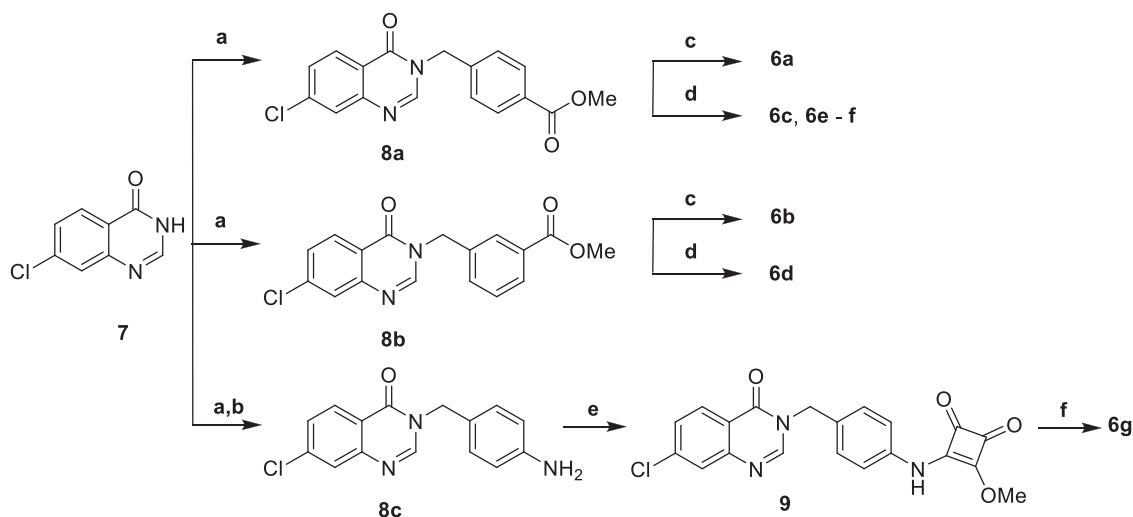
gene	Primer forward (5'-3')	Primer reverse (5'-3')
<i>HDAC1</i>	GGAATCTATCGCCCTCACA	AACAGCCATCGAATACTGG
<i>HDAC3</i>	TGTGATCGATTGGGCTGCTT	TCTGATTCTCGATCGGGTG
<i>HPRT1</i>	AGATGGTCAAGGTGCAAG	GTATTCATTATAGTCAAGGGCATATC
<i>p66Shc</i>	TCCGGAATGAGTCTCTGTCA	GAAGGAGCACAGGGTAGTGG
<i>STAT4</i>	TGCTGGCAGAGAAGCTTACA	TAGCAACAGCCGTTCTCTCT

## 2.12. Histone extraction

$1 \times 10^7$  CLL cells were harvested, washed twice with cold PBS, and lysed in Triton Extraction Buffer (TEB: PBS containing 0.5% Triton X-100 (v/v), 2 mM PMSF, 0.02% (w/v)  $\text{NaN}_3$ ) for 10 min on ice, with gentle stirring. After centrifugation ( $10000 \times g$  at 4 °C for 10 min), the supernatant was removed, and the pellet was washed in TEB buffer and centrifuged as before. Pellet was incubated overnight in 0.2 N HCl at 4 °C on a rolling table and neutralized with 2.0 M NaOH. Samples were centrifuged at  $16000 \times g$  for 10 min at 4 °C and supernatants were collected.

## 2.13. Western blot

Cells ( $5 \times 10^6$  cells/sample) were lysed in 1% (v/v) Triton X-100 in 20 mM Tris-HCl pH 8, 150 mM NaCl, in the presence of a cocktail of protease inhibitors (Calbiochem, Merck, #539134) and 0.2 mg/mL sodium orthovanadate (Merck, #S6508), for 5 min on ice. Protein and histone extracts were quantified by Quantum Protein Assay Kit (Euroclone, Milan, Italy, #EMP014500) and denatured in 4× Bolt™ LDS Sample Buffer (Thermo Fisher Scientific, Waltham, Massachusetts, #B0007) supplemented with 10× Bolt™ Sample Reducing Buffer (Thermo Fisher Scientific, #B009) for 5 min at 100 °C. Proteins were



**Scheme 1.** Synthesis of HDAC inhibitors **6a-g**. Reagents and conditions: **a**) methyl 4-(bromomethyl)benzoate for **8a** (1 eq.), methyl 3-(bromomethyl)benzoate (1 eq.) for **8b**, 1-(bromomethyl)-4-nitrobenzene for **8c** (1 eq.),  $K_2CO_3$  (2 eq.), NaI (1 eq.), 55 °C, 12 h, acetone (93–96% yield); **b**) Fe powder (10 eq.),  $NH_4Cl$  (10 eq.), EtOH, 60 °C, 4 h; **c**)  $NH_2OH \cdot HCl$  (5 eq.), methanolic KOH (5 eq.), MeOH, 25 °C, 12 h (13–24% yield); **d**) i) NaOH (4 eq.), THF,  $H_2O$ , ii) *o*-phenyldiamine (0.8 eq.) for **6c** and **6d**, *m*-phenyldiamine for **6e** (0.8 eq.), aniline for **6f** (0.8 eq.), HBTU (1.2 eq.), TEA (4 eq.), dry DMF, 25 °C, 12 h (37–73% yield); **e**) dimethyl squarate (1 eq.), MeOH, 25 °C, 15 h (47% yield); **f**) 6 N HCl, 90 °C, 14 h (87% yield).

resolved by SDS-PAGE (Life Technologies, Sarasota, Florida, USA, #NW04120BOX, #NW04125BOX) and transferred to nitrocellulose (GE Healthcare, Chicago, Illinois, USA, #9004-70-0). Immunoblots were carried out using rabbit anti-acetyl-histone H3-K9/14 (Diagenode, #C15410005), rabbit anti-histone H4 (Abcam, #ab10158), monoclonal anti-tubulin, acetylated antibody (Sigma-Aldrich, #T6793) and anti-actin (Millipore, #MAB1501) primary antibodies. Secondary peroxidase-labeled anti-mouse (#115-035-146) and anti-rabbit (#111-035-003) antibodies were from Jackson Immuno-Research. Labeled antibodies were detected using ECL kit (SuperSignal® West Pico Chemiluminescent Substrate, Thermo Scientific), and immunoblots were digitally acquired and analyzed using Alliance Q9-Atom chemiluminescence imaging system (Uvitec). Primary and secondary antibodies are listed below.

Antibodies	Host	Source	Cat. No	Dilution
anti-actin	mouse	Millipore	MAB1501	1:10000
anti-acetylated tubulin	mouse	Sigma-Aldrich	T6793	1:2000
anti-acetyl-histone H3-K9/K14	rabbit	Diagenode	A381-004	1:1000
anti-histone H4	rabbit	Abcam	ab10158	1:1000
HRP-Goat anti-mouse	goat	Jackson ImmunoResearch Laboratories	115-035-146	1:20000
HRP-Goat anti-rabbit	goat	Jackson ImmunoResearch Laboratories	111-035-003	1:20000

#### 2.14. Statistical analyses

Each experiment was performed  $\geq 3$  independent times. One-way and two-way ANOVA tests with post-hoc Tukey correction and multiple comparisons were used to compare multiple groups. One-sample Wilcoxon tests were used where samples were compared to a known standard value. Statistical analyses were performed using GraphPad Prism (RRID:SCR\_002798). Statistical significance was defined as: \*\*\*\*  $p \leq 0.0001$ ; \*\*\*  $p \leq 0.001$ ; \*\*  $p \leq 0.01$ ; \*  $p \leq 0.05$ .

#### 2.15. Computational details

##### 2.15.1. Proteins and ligands preparation

Ligands were built in Maestro suite (Maestro release 2020–3, Schrödinger, LLC, New York, NY, USA, 2020) using the available drawing tools. Compounds were minimized using MacroModel program (MacroModel release 2020–3, Schrödinger, LLC, New York, NY, USA, 2020) using OPLSAA\_2005 as force field [20]. Solvent effects were simulated by the GB/SA model with “no cutoff” for non-bonded interactions. The PRCG technique with 5000 maximum iterations (threshold for gradient convergence = 0.001) was used. The resultant structures were treated by LigPrep application (LigPrep release 2020, Schrödinger, LLC, New York, NY, 2020) to identify the most probable ionization state at physiological pH value ( $7.4 \pm 0.2$ ).

##### 2.15.2. Molecular docking

Molecular docking studies were conducted using Grid-Based Ligand Docking with Energetics (Glide) employing compounds and the protein prepared as mentioned above [21], applying Glide standard precision (SP) as a scoring function [22]. Energy grids were prepared using the default value of the protein atom scaling factor (1.0 Å) within a cubic box centered on the crystallized ligand, introducing metal-coordination constraints. The selected derivatives were docked into the selected binding site using the default parameters. The number of poses entered for post-docking minimization was set to 50. Glide SP scores were evaluated. The interactions of compounds with the selected HDAC isoforms were assessed using the ligand-interaction diagram tool available in Maestro suite. The docking protocol was validated by considering the re-docking procedure using crystallized ligands. The presented docking protocol correctly accommodated the reference ligands with a small RMSD value of the docking pose with respect to the crystallized ligands.

### 3. Results and discussion

#### 3.1. Development of compounds 6a-g

HDAC inhibitors consist of three essential elements: a surface recognition group (CAP), a zinc-binding group (ZBG), and a connection moiety among the last two elements, namely the linker (Fig. 1). In this work, the nucleus of 7-chloroquinazolin-4(3H)-one was selected as a CAP; it was further decorated with a benzyl linker, which was properly

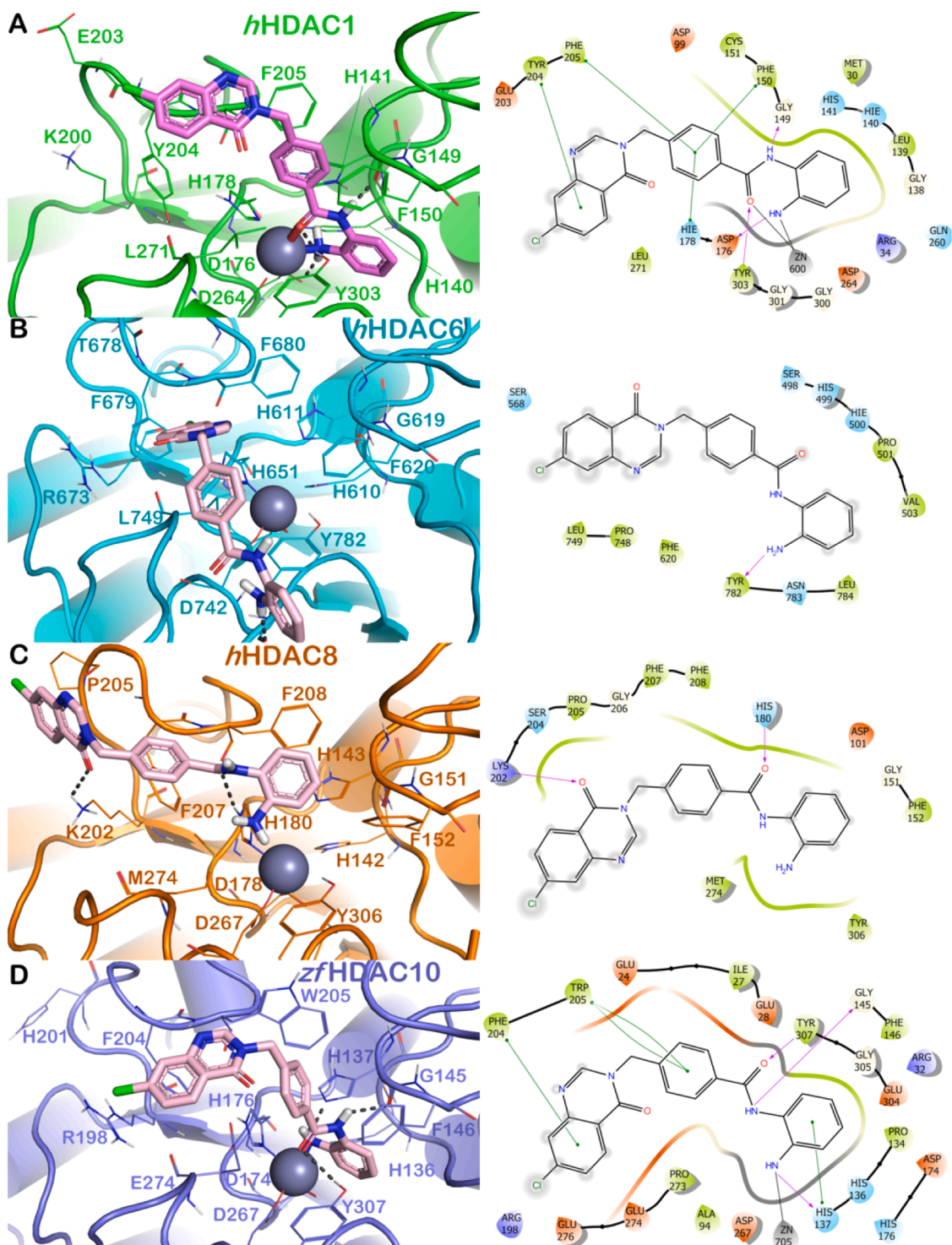


**Fig. 2.** Putative binding mode of **6c** within the binding sites of *h*HDAC1 (panel A, green cartoon; PDB ID 4BKX) *h*HDAC6 (panel B, cyan cartoon; PDB ID 5EDU) *h*HDAC8 (panel C, orange cartoon; PDB ID 3F0R), and *z*fHDAC10 (panel D, light blue cartoon; PDB ID 7U59). The residues in the active sites are represented as lines,  $Zn^{2+}$  is represented as a gray sphere. H-bonds are represented as black dotted lines. Pictures are generated by PyMOL (the PyMOL Molecular Graphics System, v1.8; Schrödinger, LLC, New York, NY, USA, 2015), while ligand-interaction diagrams were generated by Maestro (Maestro Schrödinger, LLC, New York, NY, USA, 2015).

substituted in *meta* or *para* positions with hydroxamic acids, amino benzamides or squaramic acid to obtain target compounds **6a-g** (Fig. 1, Table 1).

The synthesis of the new compounds (**6a-g**) was performed as depicted in Scheme 1.

7-Chloroquinazolin-4(3*H*)-one (**7**) was reacted with methyl 4-(bromomethyl)benzoate, 3-(bromomethyl)benzoate or 1-(bromomethyl)-4-

nitrobenzene in the presence of potassium carbonate and sodium iodide to obtain **8a-c**, respectively. **8a** and **8b** were then converted into the corresponding hydroxamic acids **6a** and **6b** by exposure to hydroxylamine hydrochloride under basic conditions.

For the synthesis of **6c** and **6d**, methyl esters **8a** and **8b** were first hydrolyzed into carboxylic acids that, without further purification, were converted into the corresponding benzamides **6c** and **6d**, in the presence



of *o*-phenyldiamine and HBTU/TEA as coupling reagents. For the synthesis of **6e** and **6f**, the carboxylic acid derived from the hydrolysis of **8a**, was treated with *m*-phenyldiamine or aniline under the same conditions described for **6c,d** to obtain **6e** and **6f**, respectively. Finally, for the synthesis of **6g**, the nitro derivative **8c** was first reduced into the corresponding aniline, which was treated with dimethyl squarate in methanol to obtain intermediate **9**. The latter compound was treated with hydrochloric acid to obtain the target compound **6g**.

### 3.2. *In vitro* HDACs inhibition profile

**6a-g** were evaluated for their ability to inhibit a selected panel of HDAC enzymes [23]. Our aim was to develop potent HDAC inhibitors to evaluate their ability to revert apoptosis defects in CLL cells, focusing our attention on class I enzymes. Specifically, we tested **6a-g** against *h*HDAC1, *h*HDAC6, *h*HDAC8, and *h*HDAC10 (Table 1). HDAC1 and HDAC8 are class I nuclear HDACs, whereas HDAC6 and HDAC10 are members of class IIB. While HDAC1 deacetylates histones and transcriptional regulators, HDAC8 is fundamentally distinct from HDAC1–3 and is the only isoform for which the gene lies on the X chromosome. Moreover, because of the similarities in the active sites of HDAC6 and HDAC8, discrimination between these two isoforms is challenging [24]. The selectivity issue among the different isoforms for HDACs is a crucial point, and our screening was directed against a panel of enzymes to identify class I selective inhibitors.

Regarding the value of screening molecules against the 11 HDAC isoforms, it has been recently pointed out that the reliability of *in vitro* enzymatic tests on all 11 HDAC isoforms is debatable [25]. For this reason, our enzymatic platform was limited to HDAC1, HDAC6 CLL-relevant isoforms, and HDAC8 and HDAC10 (CLL non-relevant enzymes) belonging to class I and IIB enzymes, respectively (Table 1).

Biochemical characterization of the new hits was preferentially performed against CLL-relevant isoforms. In particular, regarding class I enzymes (HDAC1–3,8) we performed biochemical assays of our hits against HDAC1 and HDAC8.

The first compound of the series **6a** was decorated with a hydroxamic acid in *para* position and, as expected, displayed an interesting nanomolar inhibition profile against HDAC6 ( $IC_{50} = 9.60$  nM) but also against HDAC1 ( $IC_{50} = 890$  nM) and HDAC8 ( $IC_{50} = 707$  nM). The corresponding *m*-substituted analog **6b** showed weak inhibition profiles against HDAC1, HDAC6, and HDAC8, with  $IC_{50}$  values  $> 1000$  nM.

To obtain a potentially selective HDAC1 inhibitor, the hydroxamic acid in the *p*-position of **6a** was converted into an *o*-amino benzamide, furnishing **6c**, which showed an interesting  $IC_{50}$  value of 67 nM against HDAC1 and no significant inhibition against HDAC6 and HDAC8 ( $IC_{50} > 10,000$  nM), whereas a micromolar inhibition potency against HDAC10 ( $IC_{50} = 1149$  nM) was detected. When the *o*-amino benzamide ZBG is placed at the *m*-position of the benzyl ring as in **6d**, no inhibition of HDAC1 was observed, as well as when the *o*-amino benzamide of **6c** was converted into an *m*-amino benzamide, as in **6e**. As a further SAR investigation, a monodentate ZBG was proposed as in **6f**, but also in this case the molecule was not able to inhibit HDAC1, confirming that a bidentate chelating group attached at *p*-position of the benzyl linker is necessary to inhibit HDAC1 (**6c**).

Finally, the explorative compound **6g**, presenting a squarate moiety as potential ZBG, was tested and showed limited ability to interact with the HDACs of the screening panel. Entinostat (**4**) was tested under the same experimental conditions and showed an HDAC1  $IC_{50}$  in the micromolar range, confirming compound **6c** as one of the most potent HDAC1s known to date (Table 1).

### 3.3. Computational studies

CLL-relevant class I HDAC isoforms are HDAC1 and HDAC3 together with class IIB HDAC6. These three isoforms are overexpressed in CLL cells from patients. Among class I enzymes HDAC1 activity is highly

deregulated and consequently, it is the target of our investigation.

To rationalize the high inhibitory potency of the structurally related inhibitors **6a**, **6b** and **6c** for HDAC1, HDAC6, HDAC8 and HDAC10 (Table 1), we docked them into available human enzymes crystal structures available in the Protein Data Bank (PDB) [26] (Fig. 2). Compound **6c** showed a preferential binding for HDAC1 over a panel of selected isoforms (HDAC8 and class IIB enzymes). Docking output of this compound with HDAC1, HDAC6, HDAC8, and HDAC10 isoforms highlighted the main features governing the preferential binding for HDAC1. The output is shown in Fig. 2. The key actors in this context were the use of a specific cap group combined with the *o*-amino benzamide as ZBG. While the hydroxamic acid ZBG may confer a *pan*-inhibition profile with molecules that cannot discriminate among class I and class II isoforms, the *o*-amino benzamide ZBG could potentiate interaction with CLL-relevant class I enzymes over i.e. HDAC6 (CLL-relevant) (see Table 1). Among class I enzymes, *o*-amino benzamide ZBG is crucial to obtain productive interactions with the HDAC1 binding site, maximizing the contacts with the key residues of the catalytic site throughout a bidentate coordination with the  $Zn^{2+}$  ion. Furthermore, this group could form H-bond with Gly149, Asp176, and Tyr303 residues.

Another key feature to potentiate HDAC1 binding is the benzyl linker. While the *pan* inhibitor SAHA presents a flexible alkyl spacer, the benzyl linker of **6c** establishes a strong network of hydrophobic interactions, being able to engage in three  $\pi$ - $\pi$  stacking with Phe150, His178, and Phe205. Finally, the cap group was selected to establish a  $\pi$ - $\pi$  stacking with Tyr204 (Fig. 2A). When docked into HDAC6 and HDAC8, **6c**, was not able to reach the metal centre and consequently, to properly occupy the binding sites due to the presence of the *o*-amino benzamide as ZBG. In fact, in HDAC6 (class IIB) and HDAC8 (class I), few interactions with residues Tyr782 (HDAC6) and His180 and Lys202 (HDAC8) were observed. This is reflected by the docking score values, confirmed by the reduced affinity of **6c** for HDAC6 and HDAC8 over HDAC1 isoforms (Table 1, Fig. 2B,C) (**6c** GlideScore: HDAC1 =  $-9.881$  kcal/mol; HDAC6 =  $-4.255$  kcal/mol; HDAC8 =  $-3.998$  kcal/mol; HDAC10 =  $-8.221$  kcal/mol). On the contrary, in HDAC10 catalytic site the *o*-amino benzamide was correctly accommodated in the binding site to coordinate the metal ion. Further contacts were observed with the following residues: His137 (H-bond and  $\pi$ - $\pi$  stacking), Gly145 (H-bond), Tyr307 (H-bond), Phe204 ( $\pi$ - $\pi$  stacking), and Trp205 ( $\pi$ - $\pi$  stacking). Also in this case the docking score was in agreement with the observed inhibition potency in the low micromolar range. The hydroxamic acid derivatives **6a** and **6b** did not show a remarkable selectivity profile, except for **6a**, which preferentially binds HDAC6 with an inhibitory potency in the low nanomolar range. Compound **6b** did not discriminate among the isoforms of the panel, showing  $IC_{50}$  values in the low micromolar range for HDAC1, HDAC6, and HDAC8, whereas HDAC10 is less susceptible to the inhibition with 42% inhibition at 10  $\mu$ M (**6a** GlideScore: HDAC1 =  $-8.927$  kcal/mol; HDAC6 =  $-9.385$  kcal/mol; HDAC8 =  $-9.082$  kcal/mol; HDAC10 =  $-9.280$  kcal/mol; **6b** GlideScore: HDAC1 =  $-9.579$  kcal/mol; HDAC6 =  $-9.132$  kcal/mol; HDAC8 =  $-8.560$  kcal/mol; HDAC10 =  $-8.204$  kcal/mol). In summary, the attachment of *o*-amino benzamide as ZBG in *p*-position of the benzyl linker is crucial for improving selectivity against HDAC1. Compound **6c** is one of the most potent HDAC1s known to date and this hint will be pivotal for designing the next generation of selective HDAC1s.

### 3.4. HDAC inhibitory profile of newly synthesized compounds: immunoblot analysis for the modulation of histone and non-histone proteins in leukemic cells from CLL patients

Due to their specific HDAC inhibition profile, **6a-c** were selected as tools for the evaluation of their apoptotic profile in CLL cell-based assays. In particular, **6a** was used to investigate the role of HDAC6, whereas **6c** was used to investigate the role of HDAC1; finally, **6b** was used as a non-selective HDAC inhibitor. To determine whether the



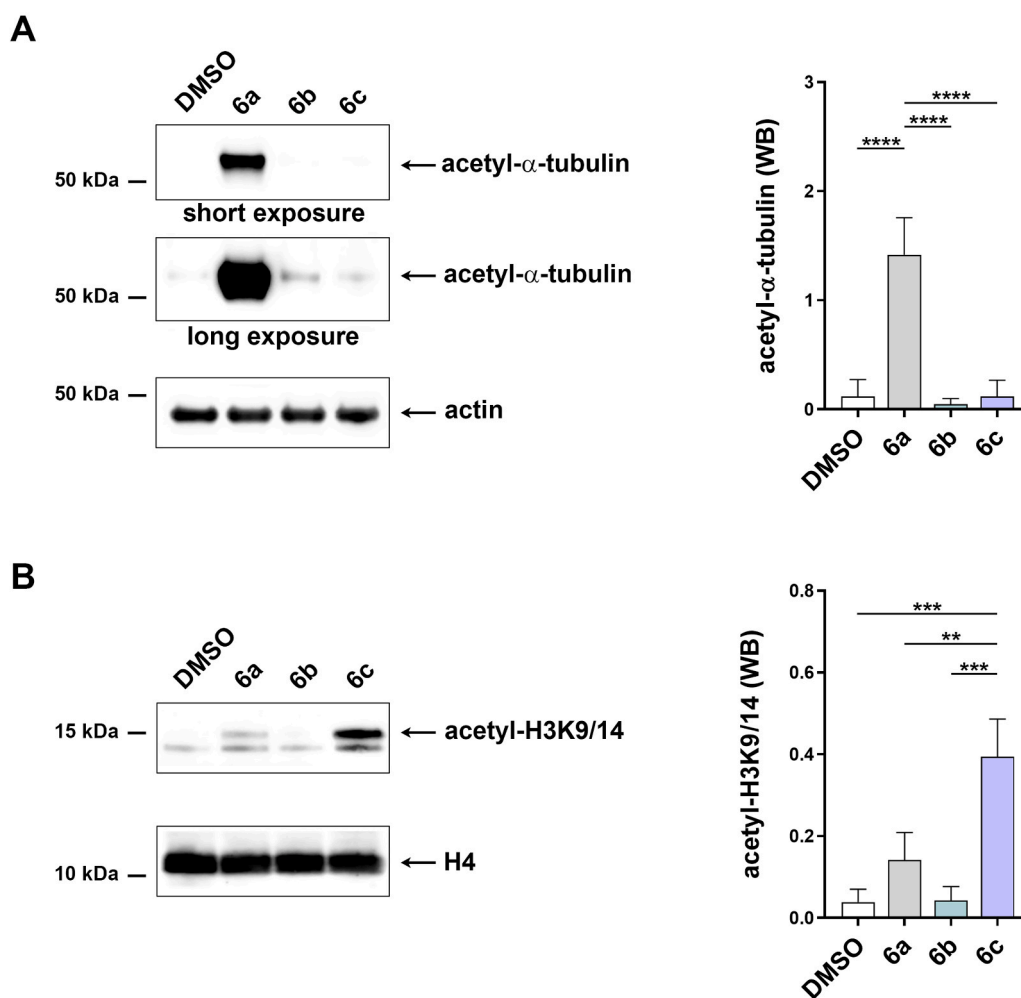


**Fig. 3.** Assessment of HDAC inhibitory activity of **6a-c** against CLL-relevant proteins. **A, B.** Immunoblot analysis of acetylated  $\alpha$ -tubulin in postnuclear supernatants (**A**) and acetylated histone H3-K9/14 in nuclear extracts (**B**) of leukemic cells isolated from peripheral blood of CLL patients ( $n=3$ ) and treated for 24 h at 37°C with 5  $\mu$ M **6a**, **6b** or **6c** compounds. The stripped filters were reprobbed with anti-actin and anti-histone H4 antibodies. Molecular weights (kDa) are indicated on the left of the panels. The quantification of three independent experiments is shown on the right. Mean $\pm$ SD. One-way ANOVA test with multiple comparison;  $p \leq 0.0001$ , \*\*\*\*;  $p \leq 0.001$ , \*\*\*;  $p \leq 0.01$ , \*\*.

selected **6a**, **6b**, and **6c** compounds displayed preferential inhibitory activity among HDACs, the acetylation levels of  $\alpha$ -tubulin (non-histone target of HDAC6 and partially of HDAC8) and H3-K9/14 (preferential histone target of HDAC1) were analyzed in CLL cells by immunoblot analyses. Leukemic cells isolated from the peripheral blood of CLL patients were treated for 24 h with either 5  $\mu$ M **6a**, **6b** and **6c** or with DMSO (**Fig. 3**).

As shown in **Fig. 3**, compound **6a** increased the acetylation levels of  $\alpha$ -tubulin (**Fig. 3A**), demonstrating its preferential inhibitory activity toward HDAC6. On the other hand, acetylation of H3-K9/14, which represents the preferential HDAC1 target, is mainly promoted by **6c**, thereby supporting its activity as HDAC1 inhibitor in CLL cells (**Fig. 3B**). Interestingly, **6a** also induced a slight increase in H3-K9/14 acetylation, although its potency in promoting  $\alpha$ -tubulin acetylation suggests that it preferentially acts on HDAC6 (**Fig. 3B**). At the same concentrations, **6b** did not elicit acetylation of either substrate (**Fig. 3**), which is consistent with its low potency and lack of selectivity toward the analyzed HDAC enzymes (**Table 1**).

### 3.5. The HDAC1 inhibitor **6c** reverts the apoptosis defect in leukemic cells from CLL patients

Leukemic cells accumulate in both peripheral blood and lymphoid

organs of CLL patients due to defective apoptosis [27]. We assessed the ability of HDACis **6a-c** to normalize CLL cell apoptosis *in vitro*. CLL cells isolated from the peripheral blood of CLL patients were treated for 24 h with 1, 2.5 and 5  $\mu$ M of **6a**, **6b** and **6c**, and apoptosis was quantified by flow cytometric analysis of the percentage of Annexin V<sup>+</sup>/PI<sup>+</sup> cells (**Fig. 4**). As a positive control, we used SAHA (**1**), whose pro-apoptotic activity in CLL cells has been previously reported [28].

As shown in **Fig. 4A**, a 24 h treatment with **6a** and **6b** compounds did not significantly affect apoptosis of CLL cells. On the contrary, treatment with the potent HDAC1 inhibitor **6c** significantly enhanced CLL cell apoptosis in a dose-dependent manner (**Fig. 4A**). Of note, the pro-apoptotic effect of **6c** was more pronounced than that of the reference pro-apoptotic *pan*-HDAC inhibitor **1** (**Fig. 4A,B**), suggesting that a preferential HDAC1 inhibition is a promising strategy to overcome the apoptosis defects present in CLL cells. Importantly, **6c** only slightly enhanced apoptosis of B cells isolated from the peripheral blood of healthy donors (HD B), suggesting that this compound has a CLL cell-specific pro-apoptotic effect (**Fig. 4B**). These results were confirmed by the significantly enhanced activation of the effector caspase-3 in CLL cells treated for 24 h with 5  $\mu$ M **6c**, but not **6a** and **6b**, as assessed by flow cytometric analysis of cells stained with the fluorescent probe NucView® 488 [18] (**Fig. 4C**). It is noteworthy that, according to the data shown in **Table 1**, at the indicated concentrations the pro-apoptotic

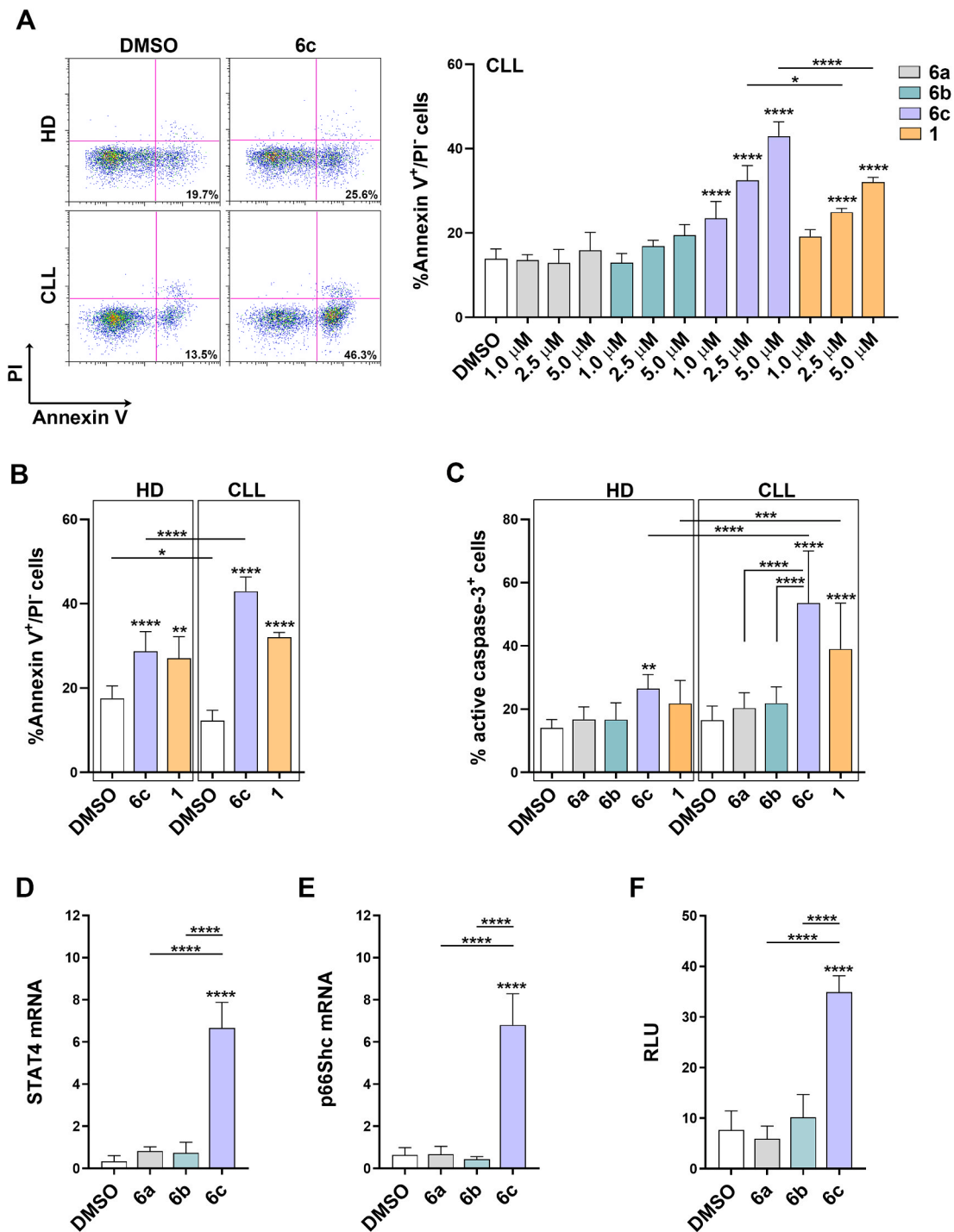


**Fig. 4.** 6c promotes apoptosis of CLL cells by enhancing STAT4 and p66Shc expression. **A.** Flow cytometric analysis of the percentage of apoptosis in leukemic cells isolated from peripheral blood of CLL patients ( $n = 4$ ) and treated for 24 h at 37°C with either 6a, 6b, 6c or 1 at the indicated concentrations. DMSO was used as control. Apoptosis was calculated as the percentage of Annexin V<sup>+</sup>/propidium iodide (PI)<sup>-</sup> cells ( $n$  independent experiments  $\geq 5$ ). **B.** Flow cytometric analysis of the percentage of apoptosis in B cells purified from buffy coats of healthy donors ( $n \geq 3$ ) and CLL patients ( $n \geq 3$ ) treated for 24 h at 37°C with either 6c or 1 at 5  $\mu$ M concentration. DMSO was used as control. Apoptosis was calculated as the percentage of Annexin V<sup>+</sup>/PI<sup>-</sup> cells ( $n$  independent experiments  $\geq 3$ ). **C.** Flow cytometric analysis of the percentage of active caspase-3<sup>+</sup> cells among B cells purified from buffy coats of healthy donors ( $n \geq 6$ ) and CLL patients ( $n \geq 4$ ) treated for 24 h at 37°C with 5  $\mu$ M of the indicated compounds. DMSO was used as control. After treatment, cells were loaded for 25 min with 5  $\mu$ M NucView® 488 active caspase-3 assay probe. Caspase-3 activation was calculated as the percentage of NucView® 488<sup>+</sup> cells. **D, E.** qRT-PCR analysis of STAT4 **D** and p66Shc **E** in leukemic cells isolated from peripheral blood of CLL patients ( $n = 4$ ) and treated for 24 h at 37°C with 5  $\mu$ M 6a, 6b, or 6c. DMSO was used as control. The relative gene transcript abundance was determined on triplicate samples using the ddCt method and normalized to HPRT1 ( $n$  independent experiments  $\geq 4$ ). **F.** Quantification of the luciferase activity in CLL cells transiently transfected with p66shc-luciferase reporter vector and then treated for 18 h at 37°C with 5  $\mu$ M 6a, 6b, or 6c. Data are expressed as relative luciferase units (RLU). Mean  $\pm$  SD. **A-E,** One-way ANOVA test with multiple comparison; **F,** Two-way ANOVA test with multiple comparison;  $p < 0.0001$ , \*\*\*\*;  $p < 0.001$ , \*\*\*;  $p < 0.05$ , \*.

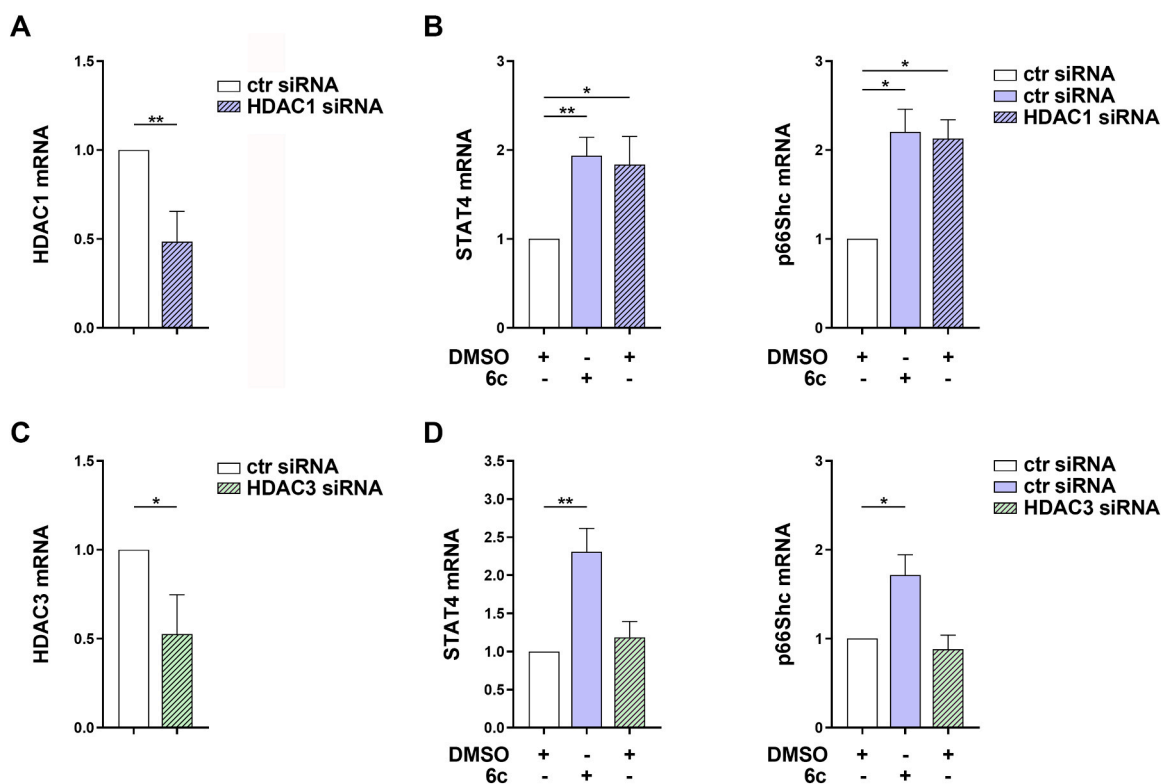


**Fig. 5.** siRNA-mediated HDAC1 depletion, but not HDAC3 depletion, enhances STAT4 and p66Shc expression. **A, C.** qRT-PCR analysis of HDAC1 (**A**) or HDAC3 (**C**) in EBV-B cells transfected with either control or HDAC1- (**A**) or HDAC3- (**B**) specific siRNAs ( $n \geq 3$ ). **B, D.** qRT-PCR analysis of STAT4 (**left**) and p66Shc (**right**) in EBV-B cells transfected as above and treated for 24 h at 37°C with either 5  $\mu$ M **6c** or DMSO ( $n \geq 3$ ). **A-D.** The relative gene transcript abundance was determined on triplicate samples using the ddCt method and normalized to HPRT1. Mean  $\pm$  SD. Paired t-test;  $p < 0.01$ ,  $**$ .  $p < 0.05$ ,  $*$ .

activity of **6c** might be in part mediated by HDAC10 inhibition. Despite this, it is also well-known that HDAC10 inhibition could affect histone H3 and  $\alpha$ -tubulin acetylation only at high doses ( $> 100 \mu$ M) in cell-based assays [29], due to a deacetylation preference for other substrates such as polyamines [30]. Hence, the data reported in Fig. 3A,B and Fig. 4A allow us to exclude the contribution of HDAC10 in the acetylation of histone and non-histone proteins and in the pro-apoptotic effect of **6c**, which can therefore be considered a specific class I HDAC inhibitor.

### 3.6. HDAC1 inhibition by **6c** (chlopynostat) restores STAT4 and p66Shc expression in leukemic cells from CLL patients

We previously reported that the impaired apoptosis shown by CLL cells is in part due to the defective expression of the pro-apoptotic adaptor p66Shc and its transcription factor STAT4 [6–8]. Since the pan-HDAC inhibitor SAHA (**1**) has been found to enhance STAT4 expression in lymphoma cells [10], we wondered whether the HDAC1 inhibitor **6c** could restore CLL cell apoptosis by normalizing the expression levels of both STAT4 and p66Shc. Leukemic cells isolated from the peripheral blood of CLL patients were treated for 24 h with 5  $\mu$ M **6a**, **6b** and **6c**, and the mRNA expression levels of STAT4 and p66Shc were quantified by RT-PCR. As shown in Fig. 4, the expression of both STAT4 and p66Shc were strongly enhanced in CLL treated with **6c**, but not with **6a** and **6b** (Fig. 4D,E).

Since STAT4 is the transcription factor of p66Shc [8], we assessed whether **6c** can influence the transcriptional activity of STAT4, therefore accounting for the enhanced p66Shc expression (Fig. 4E). To this end, leukemic cells isolated from the peripheral blood of CLL patients were transiently transfected with a construct encoding the firefly luciferase under the control of the p66shc promoter [8]. After 6 h, 5  $\mu$ M **6a**, **6b** and **6c** were added to culture media, and luciferase activity was measured after 18 h. As shown in Fig. 4F, the STAT4-dependent luciferase activity

was enhanced in CLL cells treated with **6c**, and not with **6a** and **6b** (Fig. 4F), indicating that HDAC1 inhibition enhances STAT4 transcriptional activity. Hence, preferential HDAC1 inhibition elicited by compound **6c** promotes CLL cell apoptosis by normalizing the STAT4/p66Shc proapoptotic axis.

To confirm that the pro-apoptotic effects of **6c** are mediated by its ability to inhibit the CLL-relevant member HDAC1 preferentially, HDAC1 expression was depleted by siRNA-mediated silencing in the cell line EBV-B, whose p66Shc expression is sensitive to STAT4 activation (Fig. 5A) [8].

As shown in Fig. 5A, HDAC1-KD cells showed enhanced mRNA expression of both STAT4 and p66Shc to levels comparable to those observed in EBV-B cells treated with **6c** (Fig. 5B). These data are consistent with the notion that **6c** promotes CLL cell apoptosis by preferentially inhibiting HDAC1. To further confirm this hypothesis, siRNA-mediated silencing of HDAC3, which, similar to HDAC1, belongs to the class I family of HDACs and whose expression is upregulated in CLL cells [12], was selected as a potential HDAC off-target. As shown in Fig. 5, HDAC3 siRNA (Fig. 5C) did not promote STAT4 and p66Shc expression, indicating that HDAC3 is not involved in controlling STAT4/p66Shc-dependent CLL cell apoptosis (Fig. 5D).

## 4. Conclusion

Patients with CLL exhibit defective expression of the proapoptotic protein p66Shc and its transcription factor STAT4. These defective factors induce several molecular abnormalities that impair leukemic cell apoptosis and worsen the disease. Consequently, positive modulation of p66Shc expression mediated by STAT4 activation in CLL cells may represent an attractive strategy to normalize apoptosis defects and disease progression. Direct STAT4 activation is difficult to achieve, whereas potentiation of STAT4 expression is a challenging task to be achieved by

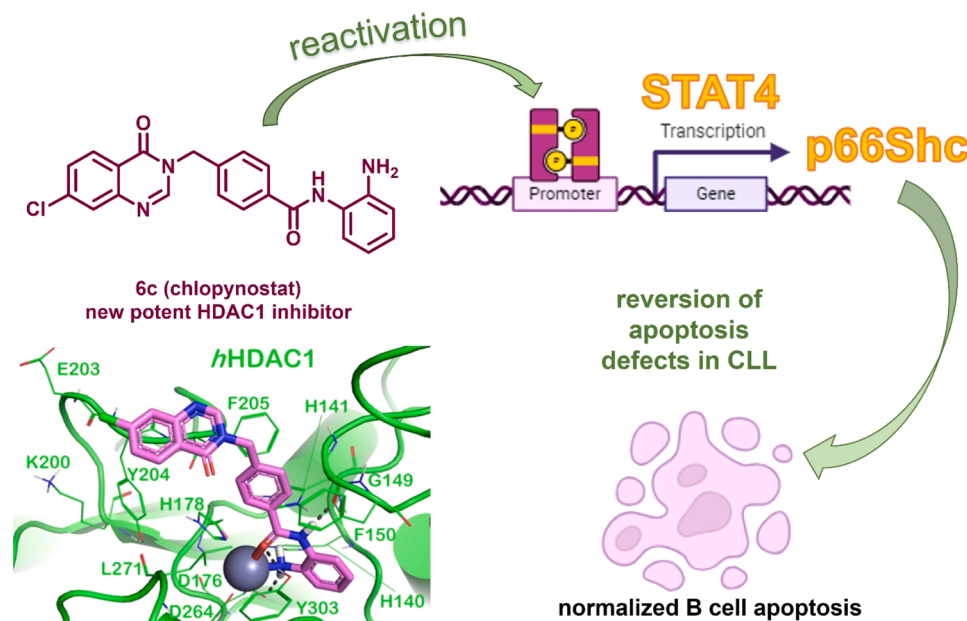


Fig. 6. HDAC1 inhibition for reversing the defective expression of STAT4/p66Shc in CLL.

modulation of nuclear enzymes. HDAC *pan*-inhibitors may positively modulate STAT4 expression in cutaneous T-cell lymphoma [10], although no data are available in CLL to date. This study elucidated the role of highly selective class I HDAC inhibitors in potentiating STAT4/p66Shc expression to reverse apoptotic machinery impairment in primary CLL cells. Entinostat (4), recognized as an HDAC1 reference inhibitor, has several drawbacks, including limited potency and selectivity; consequently, we developed the new HDAC1 inhibitor **6c** (chlodynostat) as one of the most potent and selective class I HDAC inhibitors known to date. **6c** has been used as a valuable pharmacological tool to unveil the role of class I HDAC inhibition in the positive modulation of the STAT4/p66Shc proapoptotic pathway in B cells from patients with CLL. In cell-based assays, **6c** (chlodynostat) efficiently induces apoptosis by reversing the defects in the STAT4/p66Shc proapoptotic machinery *via* HDAC1 inhibition as confirmed in HDAC1-KD and not in HDAC3-KD cells. We unveil the previously unrecognized direct involvement of HDAC1 in the impairment of the CLL apoptotic machinery and HDAC1 inhibition as a valuable strategy to reverse the defective expression of STAT4/p66Shc in patients with CLL (Fig. 6).

#### CRediT authorship contribution statement

**Monica Bocchia:** Formal analysis, Data curation. **Stefania Butini:** Writing – review & editing, Methodology, Data curation, Conceptualization. **Giuseppe Marotta:** Formal analysis, Data curation. **Sandra Gemma:** Validation, Formal analysis. **Simone Brogi:** Visualization, Supervision, Software. **Laura Patrussi:** Writing – review & editing, Writing – original draft, Methodology, Investigation, Data curation, Conceptualization. **Silvia Pasquini:** Investigation, Formal analysis, Data curation. **Gabriele Carullo:** Writing – review & editing, Writing – original draft, Validation, Investigation, Formal analysis, Data curation, Conceptualization. **Ludovica Lopresti:** Methodology, Investigation, Data curation. **Margherita Malchiodi:** Investigation. **Sara Rossi:** Validation, Investigation. **Chiara Carrara:** Formal analysis. **Vanessa Tatangelo:** Formal analysis, Data curation, Conceptualization. **Alessandro Gozzetti:** Funding acquisition, Formal analysis. **Maria Dichiarà:** Methodology, Investigation. **Martina Cappello:** Investigation. **Cosima Tatiana Baldari:** Writing – review & editing, Supervision, Project administration, Funding acquisition, Formal analysis, Data curation. **Giuseppe Campiani:** Writing – review & editing, Writing –

original draft, Project administration, Funding acquisition, Formal analysis, Data curation, Conceptualization. **Fabrizio Vincenzi:** Supervision, Methodology, Investigation. **Katia Varani:** Formal analysis.

#### Declaration of Competing Interest

The authors declare that they have no known competing financial interests or personal relationships that could have appeared to influence the work reported in this paper.

#### Acknowledgments

This work was supported by the grant Bando Ricerca Salute 2018-Regione Toscana IT - PRECISE-CLL, "Development of personalized diagnosis and innovative therapies for resistant CLL" to Giuseppe Campiani, Cosima Tatiana Baldari, Alessandro Gozzetti, Stefania Butini and Laura Patrussi.

#### Appendix A. Supporting information

Supplementary data associated with this article can be found in the online version at [doi:10.1016/j.biopha.2024.116537](https://doi.org/10.1016/j.biopha.2024.116537).

#### References

- [1] M. Hallek, O. Al-Sawaf, Chronic lymphocytic leukemia: 2022 update on diagnostic and therapeutic procedures, *Am. J. Hematol.* 96 (2021) 1679–1705, <https://doi.org/10.1002/AJH.26367>.
- [2] J. Lachaine, K. Guinan, A. Aw, V. Banerji, I. Fleury, C. Owen, Impact of fixed-duration oral targeted therapies on the economic burden of chronic lymphocytic leukemia in Canada, *Pages 4483-4498 30, Curr. Oncol.* 2023 Vol. 30 (2023) 4483–4498, <https://doi.org/10.3390/CURRONCOL30050339>.
- [3] P. Paul, G. Stüssi, A. Brusca, D. Rossi, Genetics and epigenetics of CLL, *Leuk. Lymphoma* 64 (2023) 551–563, <https://doi.org/10.1080/10428194.2022.2153359>.
- [4] O. Al-Sawaf, K. Fischer, TP53 mutations in CLL: does frequency matter? *Blood* 138 (2021) 2600–2601, <https://doi.org/10.1182/BLOOD.2021012343>.
- [5] A. Pezzicoli, C. Olivieri, N. Capitani, A. Ventura, P. Pelicci, C.T. Baldari, Expression in T-cells of the proapoptotic protein p66SHC is controlled by promoter demethylation, *Biochem Biophys. Res. Commun.* 349 (2006) 322–328, <https://doi.org/10.1016/J.BBRC.2006.08.039>.
- [6] N. Capitani, O.M. Lucherini, E. Sozzi, M. Ferro, N. Giommoni, F. Finetti, G. De Falco, E. Cencini, D. Raspadori, P.G. Pelicci, F. Lauria, F. Forconi, C.T. Baldari, Impaired expression of p66Shc, a novel regulator of B-cell survival, in chronic



- lymphocytic leukemia, *Blood* 115 (2010) 3726–3736, <https://doi.org/10.1182/BLOOD-2009-08-239244>.
- [7] L. Patrussi, N. Capitani, C.T. Baldari, P66Shc: a pleiotropic regulator of b cell trafficking and a gatekeeper in chronic lymphocytic leukemia, *Cancers (Basel)* 12 (2020), <https://doi.org/10.3390/CANCERS12041006>.
- [8] F. Cattaneo, L. Patrussi, N. Capitani, F. Frezzato, M.M. D'Elios, L. Trentin, G. Semenzato, C.T. Baldari, F. Cattaneo, L. Patrussi, N. Capitani, F. Frezzato, M. M. D'Elios, L. Trentin, G. Semenzato, C.T. Baldari, Expression of the p66Shc protein adaptor is regulated by the activator of transcription STAT4 in normal and chronic lymphocytic leukemia B cells, *Oncotarget* 7 (2016) 57086–57098, <https://doi.org/10.18632/ONCOTARGET.10977>.
- [9] A. Goropevšek, M. Holcar, T. Avčin, The role of STAT signaling pathways in the pathogenesis of systemic lupus erythematosus, *Clin. Rev. Allergy Immunol.* 52 (2017) 164–181, <https://doi.org/10.1007/S12016-016-8550-Y>.
- [10] I.V. Litvinov, B. Cordeiro, S. Fredholm, N. Ødum, H. Zargham, Y. Huang, Y. Zhou, K. Pehr, T.S. Kupper, A. Woetmann, D. Sasseville, Analysis of STAT4 expression in cutaneous T-cell lymphoma (CTCL) patients and patient-derived cell lines, *Cell Cycle* 13 (2014) 2975–2982, <https://doi.org/10.4161/15384101.2014.947759>.
- [11] J.C. Wang, M.I. Kafel, B. Avezbakiev, C. Chen, Y. Sun, C. Rathnasabapathy, M. Kalavar, Z. He, J. Burton, S. Lichter, Histone deacetylase in chronic lymphocytic leukemia, *Oncology* 81 (2012) 325–329, <https://doi.org/10.1159/000334577>.
- [12] M. Van Damme, E. Crompot, N. Meuleman, P. Mineur, D. Bron, L. Lagneaux, B. Stamatopoulos, HDAC isoenzyme expression is deregulated in chronic lymphocytic leukemia B-cells and has a complex prognostic significance, *Epigenetics* 7 (2012) 1403–1412, <https://doi.org/10.4161/EPI.22674>.
- [13] V. Ribrag, W.S. Kim, R. Bouabdallah, S.T. Lim, B. Coiffier, A. Illes, B. Lemieux, M.J. S. Dyer, F. Offner, Z. Felloussi, I. Kloos, Y. Luan, R. Vezen, T. Graef, F. Morschhauser, Safety and efficacy of abexinostat, a pan-histone deacetylase inhibitor, in non-Hodgkin lymphoma and chronic lymphocytic leukemia: results of a phase II study, *Haematologica* 102 (2017) 903–909, <https://doi.org/10.3324/HAEMATOL.2016.154377>.
- [14] R. Bichi, S.A. Shinton, E.S. Martin, A. Koval, G.A. Calin, R. Cesari, G. Russo, R. Hardy, C.M. Croce, Human chronic lymphocytic leukemia modeled in mouse by targeted TCL1 expression, *Proc. Natl. Acad. Sci. U. S. A.* 99 (2002) 6955–6960, <https://doi.org/10.1073/PNAS.102181599>.
- [15] K. Maharaj, J.J. Powers, M. Mediavilla-Varela, A. Achille, W. Gamal, S. Quayle, S. S. Jones, E. Sahakian, J. Pinilla-Ibarz, HDAC6 inhibition alleviates CLL-induced T-cell dysfunction and enhances immune checkpoint blockade efficacy in the Eμ-TCL1 model, *Front Immunol.* 11 (2020) 590072, <https://doi.org/10.3389/FIMMU.2020.590072/BIBTEX>.
- [16] G. Carullo, G. Di Bonaventura, S. Rossi, V. Lupetti, V. Tudino, S. Brogi, S. Butini, G. Campiani, S. Gemma, A. Pompilio, Development of quinazolinone derivatives as modulators of virulence factors of *Pseudomonas aeruginosa* cystic fibrosis strains, *Molecules* 28 (2023) 6535, <https://doi.org/10.3390/MOLECULES28186535/S1>.
- [17] V. Tatangelo, G. Boncompagni, N. Capitani, L. Lopresti, N. Manganaro, F. Frezzato, A. Visentin, L. Trentin, C.T. Baldari, L. Patrussi, p66Shc deficiency in chronic lymphocytic leukemia promotes chemokine receptor expression through the ROS-dependent inhibition of NF-κB, *Front Oncol.* 12 (2022) 877495, <https://doi.org/10.3389/FONC.2022.877495/BIBTEX>.
- [18] R.S. Amendola, A.C.B.M. Martin, H.S. Selistre-de-Araújo, H.A. Paula-Neto, R. Saldanha-Gama, C. Barja-Fidalgo, ADAM9 disintegrin domain activates human neutrophils through an autocrine circuit involving integrins and CXCR2, *J. Leukoc. Biol.* 97 (2015) 951–962, <https://doi.org/10.1189/JLB.3A0914-455R>.
- [19] L. Patrussi, N. Manganaro, N. Capitani, C. Olivieri, V. Tatangelo, F. Libonati, F. Finetti, F. Frezzato, A. Visentin, M.M. D'Elios, L. Trentin, G. Semenzato, C. T. Baldari, Enhanced IL-9 secretion by p66Shc-deficient CLL cells modulates the chemokine landscape of the stromal microenvironment, *Blood* 137 (2021) 2182–2195, <https://doi.org/10.1182/BLOOD.202005785>.
- [20] W.L. Jorgensen, D.S. Maxwell, J. Tirado-Rives, Development and testing of the OPLS all-atom force field on conformational energetics and properties of organic liquids, *J. Am. Chem. Soc.* 118 (1996) 11225–11236, [https://doi.org/10.1021/JA9621760/SUPPL\\_FILE/JA11225.PDF](https://doi.org/10.1021/JA9621760/SUPPL_FILE/JA11225.PDF).
- [21] G. Carullo, L. Bottoni, S. Pasquini, A. Papa, C. Contri, S. Brogi, V. Calderone, M. Orlandini, S. Gemma, K. Varani, S. Butini, F. Galvagni, F. Vincenzi, G. Campiani, Synthesis of unsymmetrical squaramides as allosteric GSK-3β inhibitors promoting β-catenin-mediated transcription of TCF/LEF in retinal pigment epithelial cells, *ChemMedChem* 17 (2022), <https://doi.org/10.1002/CMDC.202200456>.
- [22] T.A. Halgren, R.B. Murphy, R.A. Friesner, H.S. Beard, L.L. Frye, W.T. Pollard, J. L. Banks, Glide: a new approach for rapid, accurate docking and scoring. 2. Enrichment factors in database screening, *J. Med. Chem.* 47 (2004) 1750–1759, <https://doi.org/10.1021/jm030644s>.
- [23] G. Campiani, C. Cavella, J.D. Osko, M. Brindisi, N. Relitti, S. Brogi, A.P. Saraswati, S. Federico, G. Chemi, S. Maramai, G. Carullo, B. Jaeger, A. Carleo, R. Benedetti, F. Sarno, S. Lamponi, P. Rottoli, E. Bargagli, C. Bertucci, D. Tedesco, D. Herp, J. Senger, G. Ruberti, F. Saccoccia, S. Saponara, B. Gorelli, M. Valoti, B. Kennedy, H. Sundaramurthi, S. Butini, M. Jung, K.M. Roach, L. Altucci, P. Bradding, D. W. Christianson, S. Gemma, A. Prasse, Harnessing the role of HDAC6 in idiopathic pulmonary fibrosis: design, synthesis, structural analysis, and biological evaluation of potent inhibitors, *J. Med. Chem.* 64 (2021) 9960–9988, [https://doi.org/10.1021/ACS.JMEDCHEM.1C00184/SUPPL\\_FILE/JM1C00184\\_SI\\_004.XLS](https://doi.org/10.1021/ACS.JMEDCHEM.1C00184/SUPPL_FILE/JM1C00184_SI_004.XLS).
- [24] S. Federico, T. Khan, A. Fontana, S. Brogi, R. Benedetti, F. Sarno, G. Carullo, A. Pezzotta, A.P. Saraswati, E. Passaro, L. Pozzetti, A. Papa, N. Relitti, S. Gemma, S. Butini, A. Pistocchi, A. Ramunno, F. Vincenzi, K. Varani, V. Tatangelo, L. Patrussi, C.T. Baldari, S. Saponara, B. Gorelli, S. Lamponi, M. Valoti, F. Saccoccia, M. Giannaccari, G. Ruberti, D. Herp, M. Jung, L. Altucci, G. Campiani, Azetidin-2-one-based small molecules as dual hHDAC6/HDAC8 inhibitors: Investigation of their mechanism of action and impact of dual inhibition profile on cell viability, *Eur. J. Med. Chem.* 238 (2022) 114409, <https://doi.org/10.1016/J.EJMECH.2022.114409>.
- [25] T.C.S. Ho, A.H.Y. Chan, A. Ganesan, Thirty years of HDAC inhibitors: 2020 Insight and hindsight, *J. Med. Chem.* 63 (2020) 12460–12484, <https://doi.org/10.1021/acs.jmedchem.0c00830>.
- [26] A. Papa, I. Cursaro, L. Pozzetti, C. Contri, M. Cappello, S. Pasquini, G. Carullo, A. Ramunno, S. Gemma, K. Varani, S. Butini, G. Campiani, F. Vincenzi, Pioneering first-in-class FAAH-HDAC inhibitors as potential multitarget neuroprotective agents, *Arch. Pharm. (Weinh.)* 356 (2023) 2300410, <https://doi.org/10.1002/ARDP.202300410>.
- [27] T.J. Kipps, F.K. Stevenson, C.J. Wu, C.M. Croce, G. Packham, W.G. Wierda, S. O'Brien, J. Gribben, K. Rai, Chronic lymphocytic leukaemia, 3, *Nat. Rev. Dis. Prim.* 2017 3 (1) (2017) 1–22, <https://doi.org/10.1038/nrdp.2016.96>.
- [28] A. Pérez-Perarnau, L. Coll-Mulet, C. Rubio-Patiño, D. Iglesias-Serret, A.M. Cosiáls, D.M. González-Gironès, M. de Frias, A.F. de Sevilla, E. de la Banda, G. Pons, J. Gil, Analysis of apoptosis regulatory genes altered by histone deacetylase inhibitors in chronic lymphocytic leukemia cells, *Epigenetics* 6 (2011) 1228–1235, <https://doi.org/10.4161/EPI.6.10.17200>.
- [29] R.R. Steimbach, C.J. Herbst-Gervasoni, S. Lechner, T.M. Stewart, G. Klinke, J. Ridinger, M.N.E. Géraldy, G. Tihanyi, J.R. Foley, U. Uhrig, B. Kuster, G. Poschet, R.A. Casero, G. Médard, I. Oehme, D.W. Christianson, N. Gunkel, A.K. Miller, AzasAHA derivatives are selective histone deacetylase 10 chemical probes that inhibit polyamine deacetylation and phenocopy HDAC10 knockout, *J. Am. Chem. Soc.* 144 (2022) 18861–18875, <https://doi.org/10.1021/JACS.2C05030>.
- [30] Y. Hai, S.A. Shinsky, N.J. Porter, D.W. Christianson, Histone deacetylase 10 structure and molecular function as a polyamine deacetylase, 8, *Nat. Commun.* 2017 8 (1) (2017) 1–9, <https://doi.org/10.1038/ncomms15368>.